Physics of the Earth and Planetary Interiors
Volume 290, May 2019, Pages 10–19

The original publication is available at:
https://www.sciencedirect.com/science/article/pii/S0031920118303182

A seismic quiescence before the 2017 Mw 7.3 Sarpol Zahab (Iran) earthquake: detection and analysis by improved RTL method

Stefania Gentili[1], Antonella Peresan[1], Mohammad Talebi[2], Mehdi Zare[2], and Rita Di Giovambattista[3]

[1] Istituto Nazionale di Oceanografia e di Geofisica Sperimentale, OGS, Udine, Italy.

[2] International Institute of Earthquake Engineering and Seismology (IIEES), Tehran, Iran.

[3] Istituto Nazionale di Geofisica e Vulcanologia, INGV, Roma, Italy.

Abstract

A major earthquake, with magnitude Mw 7.3, struck Sarpol Zahab (Kermanshah province, Iran) on November 12 2017, causing extended damage and casualties. The epicentre was located in the Northwestern part of the Zagros mountain range, an active belt originated by the Arabia-Eurasia collision.

We explore seismicity preceding this earthquake, by using the Iranian Seismological Center instrumental earthquake catalog (IGTU), with the aim to identify possible anomalies in background seismicity that can be related with this and other future large events. For this purpose, we used a method for intermediate term forecasts of large earthquakes, namely the

Region Time Length (RTL) algorithm, which analyzes declustered catalogs and is sensitive to quiescences that may precede major earthquakes. RTL has been progressively refined and has been applied in several regions worldwide during the last decades. To decluster the earthquake catalog we used a quite novel approach, based on the nearest-neigbour distances between events in the space-time-energy domain, a method that preserves the background seismicity while removing the clustered component.

The retrospective application of RTL algorithm to the area surrounding the mainshock epicenter highlights two significant quiescences: one preceding the Sarpol Zahab Mw 7.3 earthquake, and the other occurring before a Mw 5.7 earthquake, which struck the same region on November 2013. The quiescences duration ranges from few months to one year and is compatible with earlier results from different regions of the world.

In addition, we applied an enhanced variant of RTL algorithm, which allows us drawing maps for the whole study region and that shows only quiescences consistently detected for different choices of the free parameters, and hence more stable. The resulting map for Northwestern Iran, calculated for the time span 1 June 2017 - 11 November 2017, evidences two broad quiescence regions, oriented NW-SE along the Zagros belt. One, located to the north, evidences a significant seismic anomaly corresponding to the Sarpol Zahab earthquake, which disappeares immediately after the event. The second one, located in the southeastern part of the study region, persists up to the end of the available catalog (October 4, 2018).

1. Introduction

On November 12, 2017, at 18:18 UTC, a major earthquake (Mw=7.3 Lat=34.77^{o}, Lon=45.76^{o}) occurred close to the town of Sarpol Zahab in the Kermanshah province of Iran, close to the Iran–Iraq border, causing extended damage and casualties. The region belongs to the Zagros mountain range, one of the youngest and most seismically active belts on Earth, originated by the Arabia-Eurasia collision since Late Paleogene, and extending from South-East Turkey to the south of Iran. The accommodation of the convergence between Arabia and Eurasia differs along the Zagros belt (Walpersdorf et al, 2006). Tectonically, the principal differences in parts of

Zagros are due to the orientations of major dextral faults and in their relationships with young thrusts and folds (Bachmanov et al, 2004).

Seismicity in Zagros is characterized mostly by moderate-size earthquakes (M≤6), with few sporadic events having magnitude M≥7. Most of the earthquakes occur in the lower folded-sedimentary cover; in the southern part, in particular, the weak Hormuz salt at the base of the cover confines most faulting and limits the earthquake magnitudes up to 6.0 (Nissen et al., 2011). The northern part of Zagros, including the zone affected by the 2017 Sarpol Zahab earthquake with magnitude of Mw=7.3, have experienced smaller number of earthquakes than the southern part of it. In the northern part of Zagros, the crustal deformation occurs mostly seismically, while aseismic strain dominates crustal deformation on Southern Zagros (Palano et al, 2018).

Zagros includes numerous cases of active faulting (Figure 1), such as Main Recent Fault (MRF), Main Zagros Reverse Fault (MZRF), High Zagros Fault (HZF), and Mountain Front Fault (MFF).

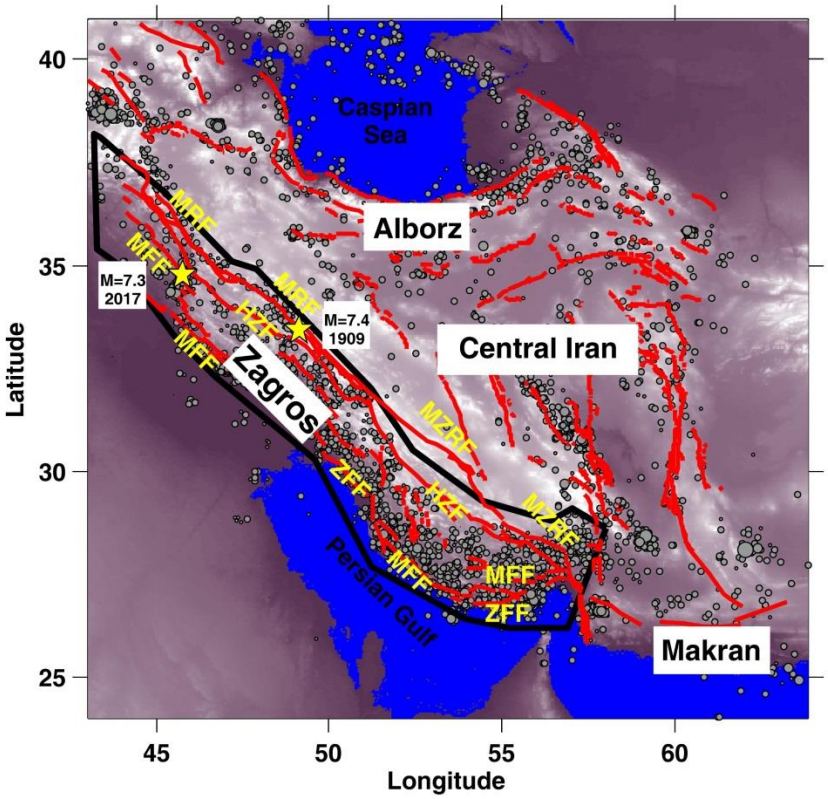

Figure 1. Major tectonic domains of the Iranian plateau including their major active faults (Hessami et al, 2003) and seismicity (IGTU data for the period 2006-2017 (IRSC, 2018)), overlaid on the topography. Black polygon and yellow stars show the Zagros region (Mirzaei et al, 1999) and instrumental large magnitude earthquakes (M≥7) along Zagros (Shahvar et al, 2013, IRSC, 2018), respectively.

A characteristic feature of the northern Zagros is that many young folds southwest of the Main Recent Fault (MRF) strike parallel or very obliquely to the fault trend (Bachmanov et al, 2004). Based on the location of destructive earthquakes in Zagros, it has been proposed that all of the big-sized events in northern part of Zagros are somehow related to the Main Recent Fault (MRF) system (e.g. Tchalenko and Broud, 1974). The 1909 Silakhor earthquake of Ms=7.4 is the largest event in the region, which has been caused by one of the segments of MRF system (Tchalenko and Braud, 1974; Bachmanov et al, 2004). However, according to the map of major active faults of Iran (Hessami et al, 2003), it can be suggested that the Mw=7.3 2017 Sarpol Zahab earthquake is probably related to the Mountain Front Fault (MFF). Using interferometric synthetic aperture radar (InSAR) data of this strong earthquake, Yang et al (2018) discussed that the seismogenic fault did not extend to the ground surface, but some shallow folds have been activated by the mainshock. It is also suggested that the significant fault slip concentrated at the depth of 10- to 14-km.

Before the occurrence of November 2017 Mw=7.3 Sarpol Zahab earthquake, it was generally assumed that such a big earthquake was not likely to occur where it did (e.g. IIEES report, 2017). This suggests that the current view of spatio-temporal behavior of seismicity in the Zagros region is still incomplete, and novel knowledge is therefore needed to study the present-day dynamics of Zagros. In this paper, we analyze the spatio-temporal trend of seismicity in Northwestern Iran.

Many studies in literature evidenced seismic quiescence before strong earthquakes in very different regions of the world (e. g. Wyss et al., 1997; Huang, 2004; Gentili, 2010, Talebi et al., 2015, Pu, 2018). The quiescence is a well-known phenomenum detected in both seismicity and laboratory experiments that has been explained by the dilatancy hardening over a broad region surrounding the nucleation zone of the impending earthquake (Scholz, 1988), by the diffusion of pore fluids during a successive crack linkage phase (Main and Meredith, 1989), by the locking of the fault segments before the mainshock (Wyss and Haberman, 1988).

In this paper, we explored seismicity preceding the Sarpol Zahab earthquake in order to verify if it has been preceded by a seismic sequence. We used the Region Time Length (RTL) algorithm (Sobolev and Tyupkin 1996, 1997), a method that has been applied in several regions worldwide (Di Giovambattista and Tyupkin, 2000, 2004; Sobolev et al., 2002; Huang, 2006; Gentili and Bressan, 2007; Huang, 2008; Mignan and Di Giovambattista, 2008; Gentili, 2010; Nagao et al., 2011; Huang and Ding, 2012; Wen et al., 2016; Gentili et al. 2017) and for which several improvements have been developed in the last years.

2. Data and declustering

The data used in this study (see Fig. 1) were extracted from the regional catalog of the Iranian Seismological Center (IGTU catalog), which is available at http://irsc.ut.ac.ir/bulletin.php (IRSC, 2018). The IGTU catalog lists events with magnitude M≥2.5, recorded in the Iranian plateau and adjacent areas since 1 January 2006.

In order to investigate the features of seismicity by RTL method, we extracted the earthquake data from January 2006 to October 2018 and selected the region surrounding Sarpol Zahab event (Northwestern Iran), within the following coordinates range: Lat=30-38°N, Lon=43-53°E.

The distribution of the number of events as a function of magnitude is shown in Fig. 2a. Different techniques have been considered to assess the threshold of magnitude completeness (Mc), based on the frequency-magnitude distribution of events (Gutenberg and Richter, 1944). However, since the distribution does not display a clear-cut bending at lower magnitudes (except for the predefined magnitude cut-off at M=2.5), the different techniques provide quite different estimates of Mc, all within the range Mc=[2.7; 3.3]. Accordingly, for the purpose of our analysis, we consider the average estimate Mc=3.0 as a reliable completeness threshold within the selected region and time span. The catalog completeness level is not affected by declustering (Fig. 2a), which is performed according to the procedure described hereinafter; moreover it keeps constant over time (see supplementary Figure S1).

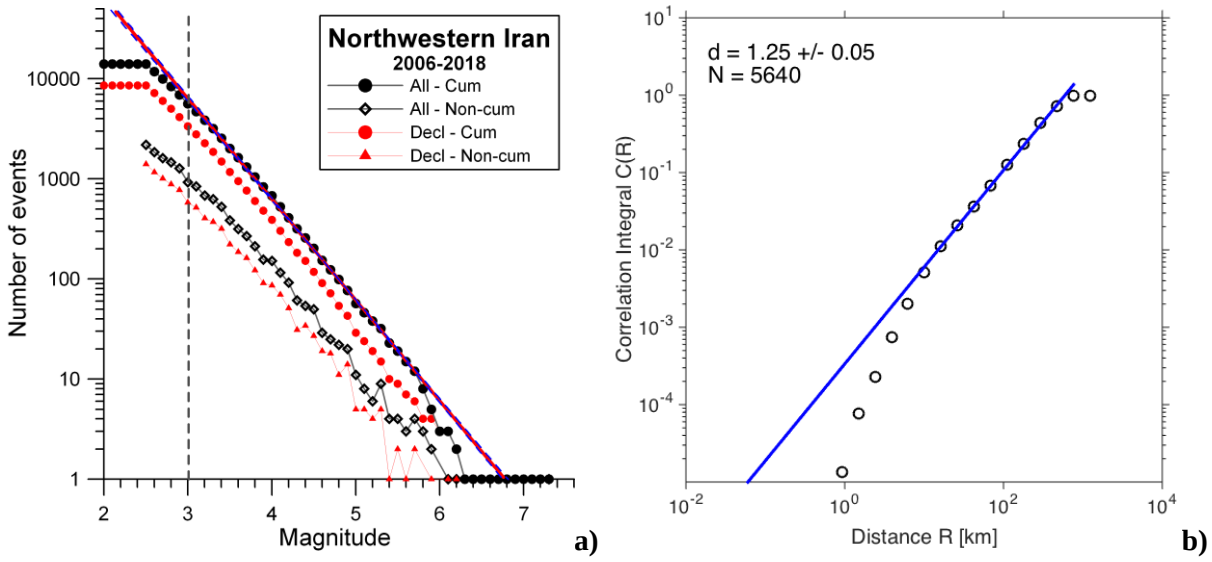

Figure 2: Completeness and scaling parameters for IGTU earthquake data in Northwestern Iran. (a) Gutenberg–Richter distribution, completeness threshold Mc=3.0 (vertical dashed line) and linear relation *LogN(M)=-bM+a* (red line), with slope *b*=0.95±0.05, obtained for events with M≥Mc=3.0. The cumulative and non-cumulative distributions of the number of events vs magnitude are shown for both original and declustered catalogs; (b) Fractal dimension *d*=D2 of earthquake epicenters from the extracted catalog with M≥3.0, computed using ZMAP6.0 software (Wiemer, 2001). The number of events with M≥3.0 is N=5640 in the original catalog, and N=3383 after declustering.

Many forecasting methods, including RTL, need as input a declustered catalog. The present analysis, the catalog declustering in particular, also requires preliminary estimation of the scaling parameters of seismicity in the area. Specifically, the *b-value* parameter of the frequency-magnitude distribution (Gutenberg and Richter, 1944) and the fractal dimension *d* (Grassberger and Procaccia, 1983) have been estimated for the selected area, using the ZMAP6.0 software (Wiemer, 2001). The robustness of the estimates has been assessed with respect to the considered time span and magnitude Mc, which allowed us to define the range of variability for the *b-value* and *d*. The obtained values are respectively: *b-value*=[0.9; 1.0] and *d*=[1.2; 1.3] (see Figure 2). It has been verified that, varying the parameters within this range, the catalog declustering does not change substantially; therefore in this study we consider *b*=0.95 and *d*=1.25.

For catalog declustering, we consider here a novel statistical approach, based on *nearest-neighbors distances* η between events in the space-time energy domain (Baiesi and Paczuski, 2004).

The nearest-neighbor distance η_{ij} between any earthquake *j* to an earlier earthquake *i* is defined as:

$$\eta_{ij} = \begin{cases} t_{ij} {r_{ij}}^{d} 10^{-bm_i}, & t_{ij} > 0 \\ \infty, & t_{ij} \leq 0 \end{cases} \quad (1)$$

where $t_{ij}=t_j-t_i$ is the inter-occurrence time, r_{ij} is the epicentral distance between the two earthquakes and m_i is the magnitude of the i^{th} earthquake.

According to Zaliapin et al. (2008), the distance η_{ij} can be also expressed as the product of rescaled time (T_{ij}) and rescaled space (R_{ij}), where:

$$T_{ij} = t_{ij} 10^{-bm_i/2} \quad (2)$$

$$R_{ij} = {r_{ij}}^{d} 10^{-bm_i/2} \quad (3)$$

The Nearest-Neighbor method for clusters identification (Zaliapin et al., 2008; Zaliapin and Ben-Zion, 2013), relies on the observation that the 1D empirical distribution of the nearest-neighbor distance η, as well as the 2D density map of its rescaled time and space components *(T,R)*, which are obtained for real seismicity, are prominently bimodal (e.g. Fig. 3). This bimodality is used to separate the earthquakes into background and cluster populations (Zaliapin and Ben-Zion, 2013), which are both unimodal, but with the clusters population centered on much shorter space-time distances. Accordingly, clusters are formed by events whose nearest-neighbor distances are smaller than a specified threshold η_0; such threshold can be selected based on the 1D distribution of η (Fig. 3a), defining a boundary between the two modes (associated with clustered and background events, respectively), and corresponds to a line with slope -1 in the 2D density map (Fig. 3b). By dropping all connections associated with large nearest-neighbor distances (i.e. $\eta_{ij} > \eta_0$) it is possible to identify individual earthquake clusters, and thus remove the related aftershocks from the catalog.

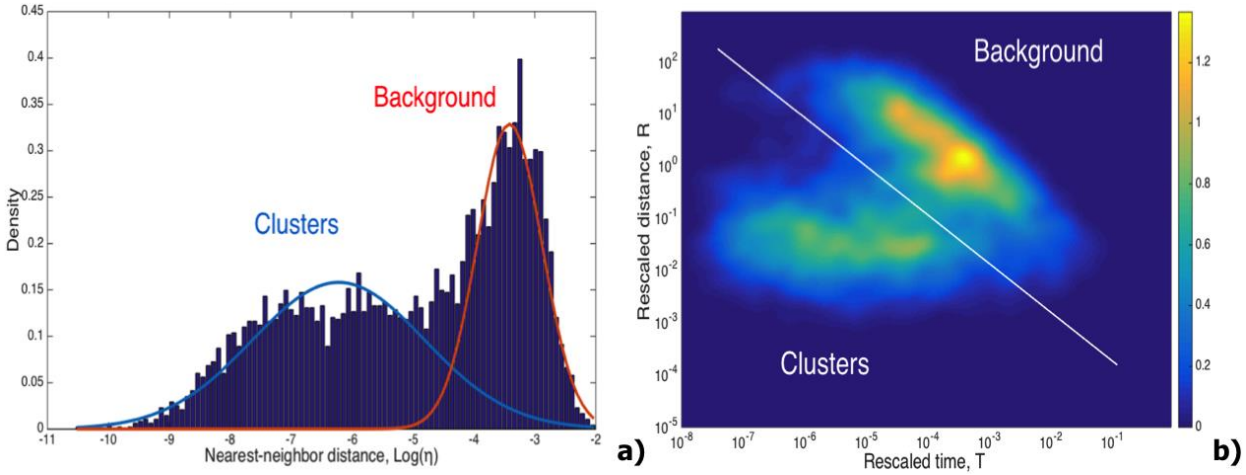

Figure 3: Nearest-neighbor method applied to Northwestern Iran: a) 1D density distribution of η, with estimated Gaussian densities for clustered (blue) and background (red) components; b) 2D joint distribution of rescaled space and time distances *(R,T)*. Adopted scaling parameters: *b=0.95* and *d=1.25*, obtained for M≥Mc=3.0 events from 2006 to October 2018.

The selection of the appropriate threshold η_0 depends on the analyzed area. When the two modes in the 1D empirical distribution are well defined, then the threshold η_0 can be automatically identified, for instance following a criterion based on a 1D Gaussian mixture model with two modes, where η_0 is the maximum likelihood boundary between the two modes (e.g. Zaliapin and Ben Zion, 2013). When one of the two modes is dominant, and the other one is less defined, a manual threshold can be more conservative (e.g. Peresan and Gentili, 2019). In Northwestern Iran, the distribution of η_{ij} values (Fig. 3b) is characterized by a prominent background component (right peak) and by a much less pronounced clustered component (left peak), which complicates the identification of the appropriate threshold η_0 separating the two components. Because of the significant overlapping and unclear separation between the two modes, for this region the threshold distance is manually set to a rather conservative threshold distance η_0, namely $\log_{10}(\eta_0)$=-5.0 (Zaliapin et al., 2008; Peresan and Gentili, 2018). By selecting this threshold distance, we preserve as much as possible the background seismicity (i.e. red curve in Fig. 3a) while removing the clustered component.

As shown by Peresan and Gentili (2019), the nearest-neighbor technique provides a robust, data-driven tool for catalogs declustering, which does not alter the features of inhomogeneous and possibly non-stationary background seismicity (Fig. 4), a property essential for this and other

similar studies. Compared to widely used methods for stochastic declustering, such as those based on ETAS model that has been recently applied to the territory of Iran (Davoudi et al., 2018), the nearest-neighbor method turns out fairly effective in clusters identification (e.g. Varini et al., 2018). Still, the method adopted here is characterised by a softer parametrisation and it is less sensitive to the completeness level of the input catalog (Peresan and Gentili, 2018), all features that are relevant for a timely application in the framework of a routine prospective analysis of seismicity patterns.

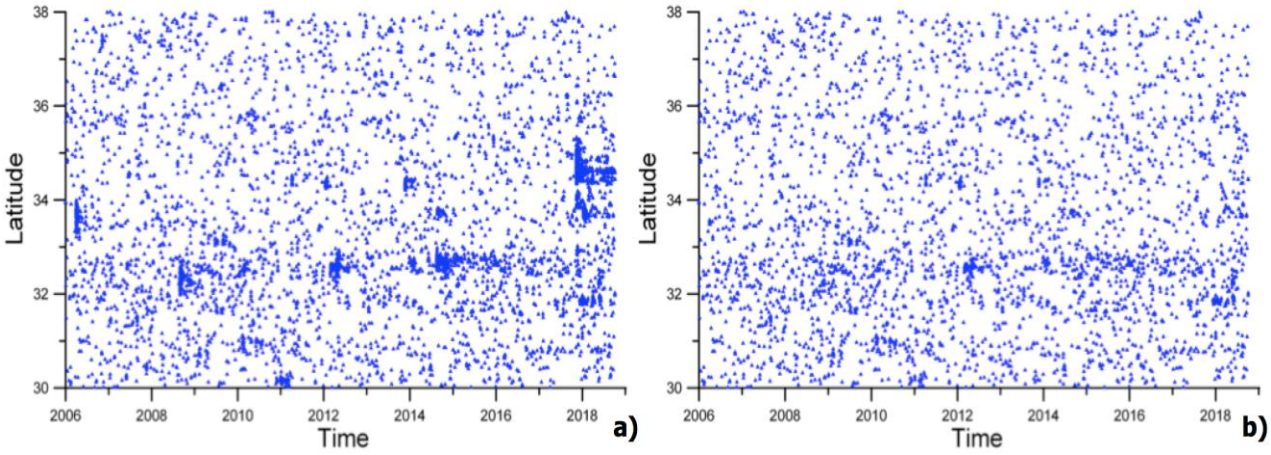

Figure 4: Space-time pattern of earthquakes occurrence in Northwestern Iran, considering: a) All events and b) Declustered catalog, with aftershocks identified by the nearest-neighbor method. Only earthquakes with M≥Mc=3.0 in the range: Lat=30-38°N, Lon=43-53°E are included in the analysis. The parameters used for declustering are: $b=0.95$, $d=1.25$ and $\log_{10}(\eta_0)$ =-5.0.

3. RTL

The Region-Time-Length function (RTL) (Sobolev et al., 1997; 1996) measures the level of seismic activity at a given location (x,y) as a function of time t. It analyzes the number of earthquakes, their size, and their distance from (x,y) within a moving time window.

The RTL function is defined by using the three functions, defined in a circular window of radius $2r_0$ from (x,y), during a time period of $2t_0$ ending at time t.

$$R(x,y,t)=\sum_{i=1}^{n}\exp\left(-\frac{r_i}{r_0}\right)-R_s(x,y,t) \tag{4}$$

$$T(x,y,t)=\sum_{i=1}^{n}\exp\left(-\frac{t-t_i}{t_0}\right)-T_s(x,y,t) \tag{5}$$

$$L(x,y,t)=\begin{cases}\sum_{i=1}^{n}\left(\frac{l_i}{r_i}\right)-L_s(x,y,t) & if \quad r_i>\varepsilon \\ \sum_{i=1}^{n}\left(\frac{l_i}{\varepsilon}\right)-L_s(x,y,t) & if \quad r_i\le\varepsilon\end{cases} \tag{6}$$

where r_i is the distance between (x,y) and the epicenter of the i^{th} earthquake, t_i is the time of occurrence of the i^{th} event, l_i is the source size of the i^{th} earthquake. Usually the source size l_i is derived from the earthquake magnitude M_i using available empirical relationships. In this paper we use the empirical equation proposed by Di Giovambattista and Typkin (2000), namely: $\log(l_i)=0.44M_i-1.289$. The parameter ε was explicitly introduced for the first time by Di Giovambattista and Tyupkin (2004); ε corresponds to the accuracy in epicenter location: since low values of r_i largely increase L (it diverges for $r_i=0$), all the earthquakes within ε are treated as if their distance was ε from the epicenter. r_0 and t_0 are parameters of the functions R and T that model their shape; in addition, they control the extent of the space and time windows, within which earthquakes are considered. The quantities R_s, T_s, and L_s are the long-term averages of these functions (linear trend corrections).

The function RTL is defined as:

$$RTL(x,y,t)=\frac{R(x,y,t)}{\sigma_R}\cdot\frac{T(x,y,t)}{\sigma_T}\cdot\frac{L(x,y,t)}{\sigma_L} \tag{7}$$

where $\sigma_R,\sigma_T,\sigma_L$ are the standard deviations of the corresponding functions. Decreases of seismic activity in terms of number, or energy, or closeness to *(x,y)* of earthquakes (hereinafter referred as *quiescences*) correspond to negative values of RTL. On the contrary, if the earthquakes' number, or their energy, or their closeness increases, then the function RTL is positive. It is important to remark that some methods (e.g. Z, Wiemer and Wyss 1994; Console et al. 2000) for seismicity analysis use only the number of earthquakes; accordingly, a "quiescence" means just a

decrease in the number of events. For RTL method, an extended meaning of quiescence is involved, because it uses also the information on earthquakes' energy and position in space.

The specific selection of the parameters r_0 and t_0 affects the shape of the RTL, because of the different time and space window considered and of the different shape of the R and T functions. Small values of radius and t_0 may capture seismicity changes close to (x, y, t); however RTL may be instable due to the poor statistics involved. Large values of the parameters, vice-versa, are more stable, but they can merge together seismicity not tectonically related.

In order to obtain the more stable results, Chen and Wu (2006) proposed a formal procedure for the identification of the most stable parameters values, based on the correlation coefficient over pairs of the RTL functions estimated using different parameters. Their method analyses r_0 and t_0 separately. In the following years, Huang and Ding (2012), proposed an integrated map of the quality of parameters. They select an area into the r_0-t_0 space where at least 70% of the correlation coefficients over pairs exceed a specified threshold for r_0 and t_0 (here and after "search area") and they calculated the best parameters inside this area as a weighted mean inside the search area.

Usually the analysis is carried out retrospectively, for a specific point (x, y) fixed at a large earthquake's epicenter and the best parameters are selected for that point. However, it is interesting to study what happens in the whole region around the epicenter, in order to evaluate the spatial dimensions of the quiescence region.

Many authors already evaluated RTL on a map (i.e. a grid of points) before a strong earthquake in retrospective analysis (Huang et al., 2001, Sobolev 2000, Di Giovambattista and Tyupkin 2000 and 2004, Huang et al. 2002, Huang 2004 and 2006). In order to do this, the RTL is first applied in the epicenter, the best r_0 and t_0 values are selected, and a time window containing the quiescence (if any) is defined. Then the whole region is sampled by a grid, the RTL is evaluated at each node of the grid by using the r_0 and t_0 optimized for the epicenter, obtaining 2D information about RTL. For each node, the function RTL vs time is summarized into a numerical feature, and the corresponding values are mapped. In some cases, the mapped feature is the minimum of the RTL in the quiescence time window (RTL_{min} - see e.g. Sobolev 2000, Di Giovambattista and Tyupkin 2000 and 2004) or, in most recent papers, the Q parameter, which is

defined as the mean of the RTL in the considered time window (Huang et al. 2002, Huang 2004, 2006). For a detailed description, see Gentili (2010).

This approach has the disadvantage that it uses the values of r_0 and t_0 optimized for the mainshock coordinates, which could be not very stable for the other nodes of the grid. In order to overcome this problem, we propose a novel approach in which only quiescences found by different values of r_0 and t_0 parameters are considered. Specifically:

1. A range of values of r_0 (r_{01}, r_{02},… r_{0M}) and t_0 (t_{01}, t_{02},… t_{0N}) is selected based on geometric/statistic/tectonic information.
2. The area is sampled by a grid, and, for every node, for every value r_{0i} and t_{0j} of the parameters value of $Q_{ij}=Q(r_{0i},t_{0j})$, is computed.
3. Only negative values of Q are considered i.e.

$$\tilde{Q}_{ij} = \begin{cases} -Q_{ij} \; if \; Q_{ij} < 0 \\ 0 \; otherwise \end{cases} \tag{8}$$

4. The geometric mean of $\tilde{Q}_{ij}$ is evaluated:

$$\hat{Q}_{ij} = -\left(\prod_{i,j} \tilde{Q}_{ij}\right)^{\frac{1}{MxN}} \tag{9}$$

Figure 4 shows a schematic representation of the proposed method.

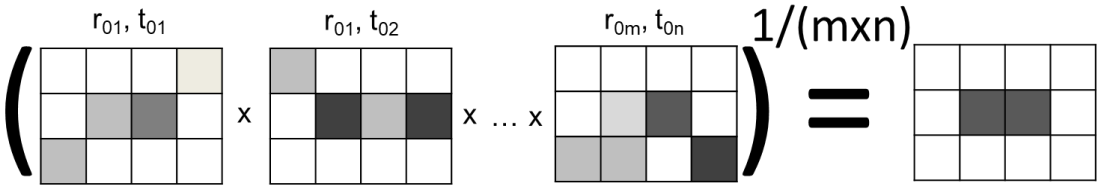

Fig. 4: Schematic representation of the proposed method. Black squares correspond to quiescences while white one correspond to 0 or positive (set to 0) values of RTL

This method reduces the number of cells with negative values of RTL respect to the ones of a map with two selected parameters. In other words, it outlines only the parts of the map where a

rather stable quiescence is detected independently on parameters. Most of the papers available in literature (e.g. Sobolev 2000, Di Giovambattista and Tyupkin 2000 and 2004, Huang et al. 2002, Huang 2004, 2006) show maps with negative values of the RTL, i.e. maps of seismic quiescence, before strong earthquakes. Gentili (2010), using the RTL method, analyzed the seismicity preceding the twelve earthquakes with magnitude larger than five in Italy from 1994 to 2004 and found a quiescence in 92% of the cases. Therefore, in this study we focus our analysis on seismic quiescence. In the original papers on RTL, the method was applied to a single point (x, y), corresponding to the coordinates of a strong earthquake epicenter. By analyzing RTL changes in time, this method emphasized not only a decrease of RTL, corresponding to a seismic quiescence around that point, but also a recovery stage from the quiescence to the background level, corresponding to a foreshock activation. Similarly, Tzanis and Vallianatos (2003) studying the Hellenic Arc, found both acceleration and deceleration of seismicity simultaneously but in separate spatial windows, while an acceleration of seismicity before the L'Aquila (in Central Italy) earthquake was detected by De Santis et al. (2010). The possible occurrence of precursory accelerating seismicity within a quiescence area is described by the Non Critical Precursory Accelerating Seismicity Theory (Mignan, 2008). In particular, Mignan and Di Giovambattista (2008) have shown this behavior in the case of 1997 Mw=6 Umbria-Marche (in Central Italy) earthquake, by analyzing the seismicity inside the quiescent region detected by RTL. However, the quiescence turns out to be a more general pattern and can be more robustly detected, particularly in a RTL map (e.g. by a mean in time or detecting the minima); further studies may permit to identify zones of accelerating seismicity within the detected quiescence regions.

4. Results

We analyzed the seismicity of Northwestern Iran (Lat=30-38°N, Lon=43-53°E) in the 10 years before the 12 November 2017 at 18:18 UTC Mw=7.3 Sarpol Zahab earthquake (Lat=34.770°N, Lon=45.760°E). The analysis in the earthquake epicenter, by using the Huang and Ding (2012) method, allowed to determine the parameters r_0 and t_0 leading to the more stable values of RTL for the epicenter itself. In Fig. 5 the quality of the parameters, i.e. the percentage of correlation coefficients over pairs exceeding a threshold is shown in color in r_0-t_0 space. In order to take into account the lower correlation of RTL if we change r_0 instead of t_0, we used the thresholds for correlation coefficients of Chen and Wu (2006), corresponding to 50% and 80% of the

correlation coefficients for r_0 and t_0 respectively (see Gentili et al. 2017). Since the signals are more correlated in this Iran application respect to e.g. Italy and Japan ones (see Gentili et al. 2017 and Huang and Ding, 2012) we selected the search area as the one where at least the 90% of the correlation coefficients over pairs exceeds the threshold for r_0 and t_0. Figure 5 shows the automatic values proposed by Huang and Ding (2012) method; the parameters are very close to the ones we adopted: r_0=45 km and t_0=1.7 years.

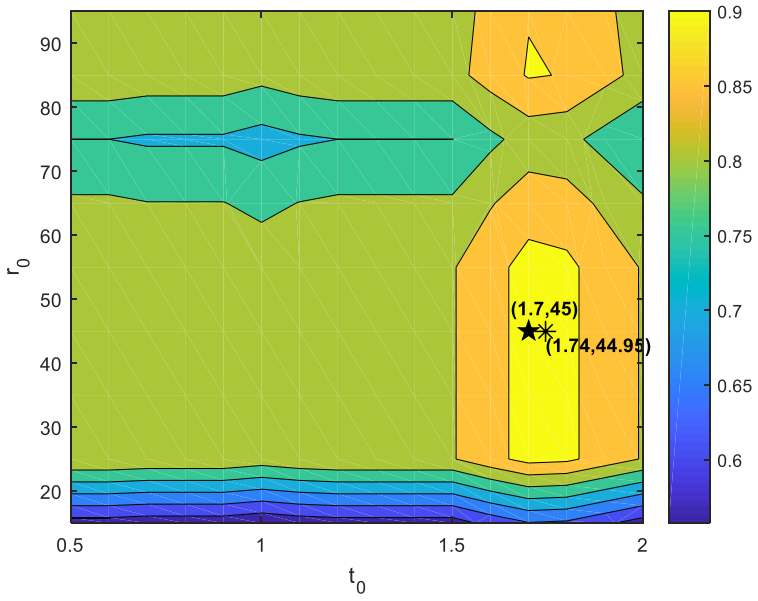

Fig 5: Map of the quality of parameters in the epicenter (Huang and Ding, 2012). Asterisk: Huang and Ding method optimal parameters. Star: selected parameters.

Figure 6 shows RTL evaluated in Sarpol Zahab earthquake epicentre till the midnight before the mainshock for the selected parameters r_0 and t_0 (red line). A first quiescence (negative values of RTL) can be detected from February 12, 2013 to November 19, 2013 and a deeper quiescence can be seen from June 12, 2017 until the mainshock time (November 12, 2017). For comparison, the RTL obtained with different parameters are shown. In particular, in Fig. 6a t_0 is set to 1.7 years and r_0 is changed, while, vice-versa, in Fig 6b r_0 is set to 45 km and t_0 is changed.

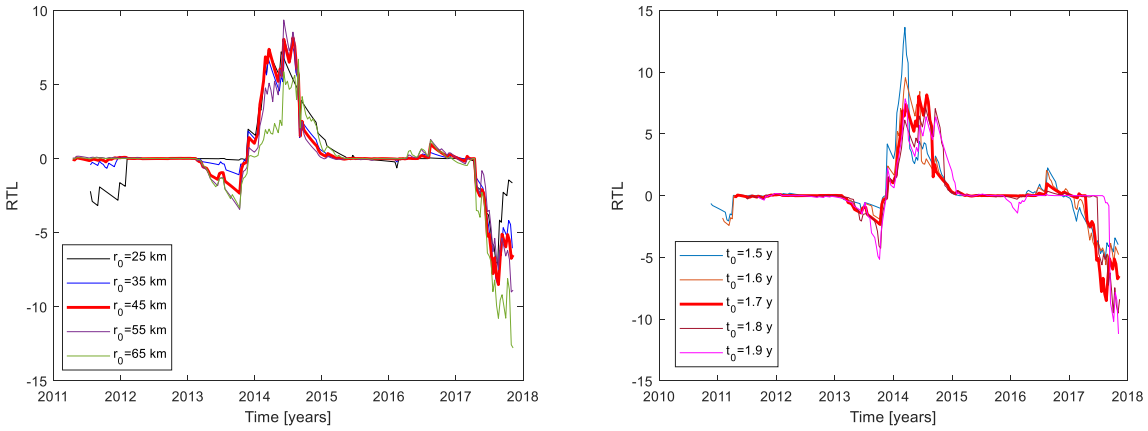

(a) (b)

Fig. 6: RTL in earthquake epicenter for different values of r_0 and t_0 parameters. Red line: selected parameters r_0=45 km and t_0=1.7 years. Other lines: (a) t_0=1.7 years and different values of r_0; (b) r_0=45 km and different values of t_0

We detect the two quiescences for all the considered values of the parameters, except for r_0=25 km, which does not show the first quiescence. The beginning of the second quiescence depends on the value selected for t_0, ranging from December 7, 2016 for t_0=1.5 years, to July 27, 2017 for r_0=1.9 years (see Fig. 5b), however it can be identified by all choices of the parameters.

While the second quiescence is clearly related, as expected, to the Mw=7.3 Sarpol Zahab strong earthquake and can be explained by a physical mechanism (see Introduction), we investigate the seismicity in the region in order to understand if a similar mechanism can be associated also to the first quiescence. Fig. 7 shows the earthquakes that occurred in the region since 2006, with the strongest events marked by a star. A 200 km radius from the mainshock is drawn. In particular, on November 22, 2013 a Mw=5.7 earthquake (Lat=34.29°N, Lon=45.56°E), struck the same area, 65 km away from 2017 mainshock epicentre; this earthquake occurred immediately after the end of the first quiescence. The distance is compatible with the detection of a quiescence using r_0 parameters such that $2r_0$>65km and the end of the quiescence corresponds to the last evaluation of RTL before the earthquake (RTL is calculated at 10 days steps). Therefore, both the quiescences in the area can be related to a process of preparation of strong events in the region.

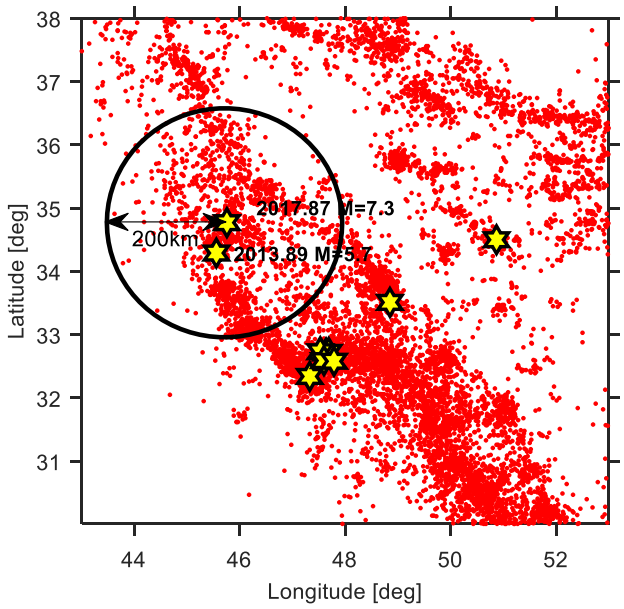

Fig. 7. Red dots: Seismicity in the Northwestern Iran from 2006 to the time of Sarpol Zahab mainshock. Yellow stars: Earthquakes with M≥5.7. The circle is centered into the Sarpol Zahab earthquake epicenter and has 200 km radius.

In order to compare RTL results with those provided by a basic descriptions of seismicity, we mapped the number of earthquakes with magnitude M≥Mc within circles of radius 90 km (corresponding to $2r_0$) in a time window of 3.4 years (corresponding to $2t_0$), centred at the nodes of a grid 20 km spaced (EN Maps).

Fig. 8 shows the difference between two EN Maps ending respectively at the end and at the beginning of the quiescences identified by RTL. Figure 8a refers to the quiescence before November 22 2013 earthquake, Figure 8b to the one before November 12, 2017 one. Both figures display negative values (dark areas) around the corresponding mainshock epicenters (marked by stars), corresponding to a decrease in the number of earthquakes.

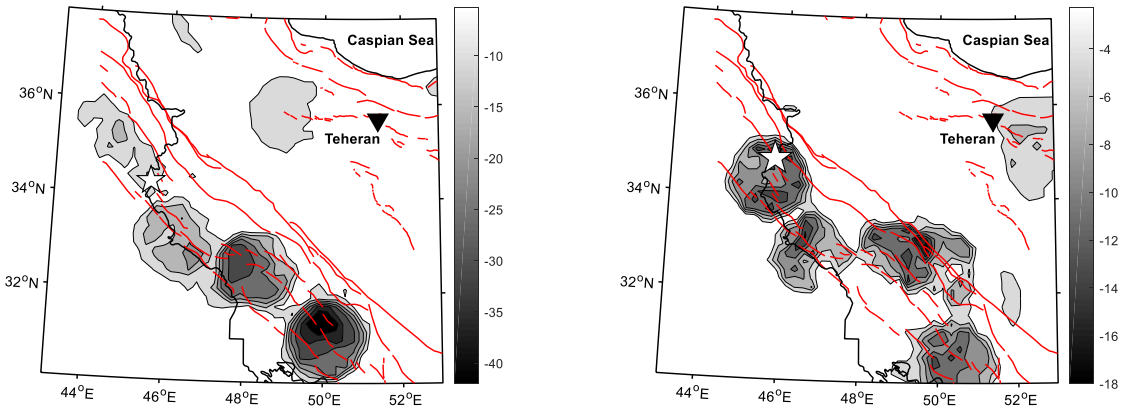

(a) (b)

Figure 8: Map of the differences between the numbers of earthquakes (EN), observed within circles of $2r_0$ km in a $2t_0$ years' time window, at two different time moments. (a) Difference between EN maps with ending time on November 22, 2013 and on February 12, 2013 (first quiescence), respectively; (b) Difference between EN maps with ending time on November 12, 2017 and on June 12, 2012 (second quiescence). Red lines: faults of the region.

In order to systematically analyze RTL over the whole region, the area is sampled by a grid 10x10 km, and, for every node, the $\hat{Q}$ value is calculated from June 23, 2016 (beginning of the quiescence for the selected r_0 and t_0) to the midnight before the mainshock. The analysis is performed with r_0 ranging between 30 to 60 km, at steps of 10 km, and t_0 ranging from 1.6 to 1.9 years, at steps of 0.1 years. We choose this range of r_0 in order to have enough statistical information (not too small radii) but to avoid confusion with the nearby Central Iran and Alborz fault seismicity. We selected the range of t_0 so as to have a sufficient statistics, while avoiding to mix up processes of preparation of different earthquakes. Moreover, the two ranges fall within the orange/yellow region of Fig. 5, corresponding to a percentage ≥85%. In order to obtain stable values of RTL, it is estimated only at the nodes where at least 10 events are reported within the considered space and time window, depending on the parameters r_0 and t_0. This condition must be satisfied for every choice of r_0 and t_0, otherwise the value of RTL at the node is set to zero. This rule automatically excludes from the analysis the areas where the seismicity is too low. In the specific case of the study region, the areas encompassing Alborz and Zagros Mountain ranges could be analyzed, due to the high level of seismicity. However, we remark that nodes of

the grid very close to the borders of catalog selection area (i.e. with distance smaller than $2r_{0M,}$ where r_{0M} is the maximum value of r_0 used into the map) may have incomplete information (border effect).

The values of $\hat{Q}$ are shown in Figure 9a; darker color corresponds to lower values of $\hat{Q}$. Fig. 9a shows also the main faults of the region (red lines) and the main earthquakes. In particular, data before 1900 are obtained by Historical Iran earthquake catalog (Ambraseys and Melville, 1982; Zare et al, 2014), data from 1900 to 2006 from Instrumental Iran Catalog (Shahvar et al, 2013) and data from 2006 to the displayed data from IGTU catalog (IRSC, 2018). Fig. 9a shows seismic quiescence anomalies extending throughout a broad region NW-SE oriented corresponding to Zagros Mountains (see Fig. 1). In particular, two quiescence regions can be detected, one located to the north and one to the south. The area around the M7.3 earthquake epicenter exhibits a significant seismic anomaly corresponding to the northern quiescence region.

From the comparison with Fig. 8b, we can see that both regions are characterized by a decrease of the number of earthquakes. The main difference between Fig. 8b and Fig. 9a is that when the improved RTL method is applied the quiescence regions are smaller. This is because RTL uses also information on energy and earthquakes' spatial distribution, besides the earthquake number. Moreover, the geometric mean of maps obtained using different parameter values takes into account only quiescence regions detected for all the selected parameters values.

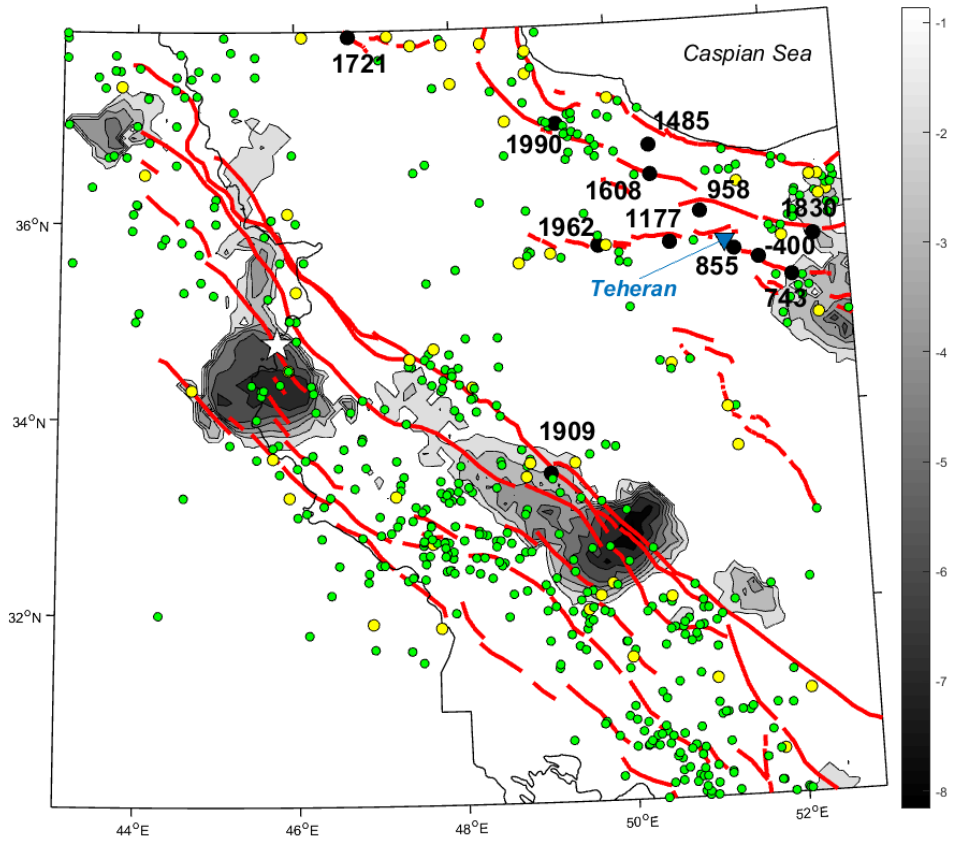
Caspian Sea
1721
1485
1990
1608
958
1830
1962
1177
-400
855
Teheran
743
1909
36°N
34°N
32°N
44°E
46°E
48°E
50°E
52°E
-1
-2
-3
-4
-5
-6
-7
-8

(a)

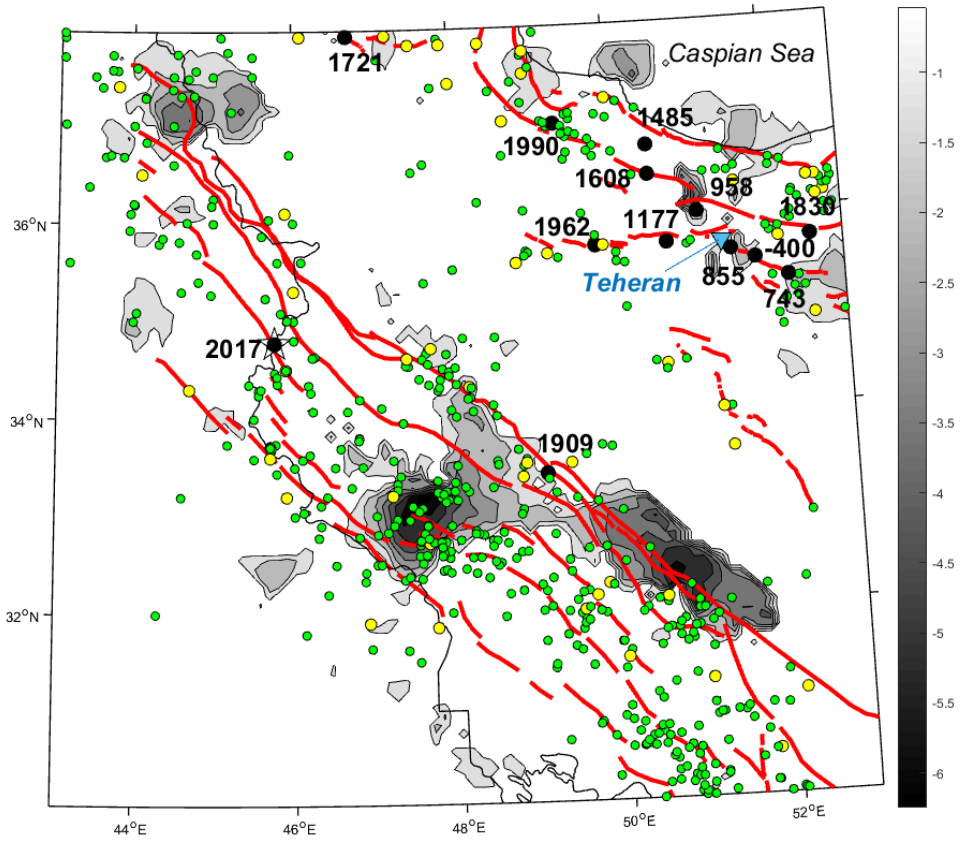

(b)

Fig.9: $\hat{Q}$ value estimates in Northwestern Iran. (a) $\hat{Q}$ value from June 12, 2017 to the midnight before the mainshock. (b) $\hat{Q}$ value from November 13, 2017 to October 4, 2018. Dark color corresponds to low values of $\hat{Q}$. Circles show the earthquakes in the area (Ambraseys and Melville, 1982 ; Shahvar et al, 2013; Zare et al, 2014; IRSC, 2018) from year -550 and till the day of the map computation: black M>=7, the year of the earthquake is shown beside; yellow 6<=M<7; green 5<=M<6. Red lines: faults.

In order to investigate how RTL function changes after the Sarpol Zahab earthquake in the whole region, we analyzed the RTL starting from the day after the mainshock and up to the end of the available catalog (October 4, 2018, see Fig. 9b). We observe that after November 12nd, the region around Sarpol Zahab earthquake epicenter is no longer quiescent. This result is not obvious, and could be achieved thanks to the declustering method applied in this study, which

preserves background seismicity (see Fig. 4). In fact, the increase of seismic activity following Sarpol Zahab earthquake does not explain the end of the quiescence, because the used catalog is declustered. On the other side, using a standard window-based declustering method, would have created gaps (see Peresan and Gentili, 2019), removing all the earthquakes in the window and introducing spurious quiescence. While the northern quiescence disappears, the quiescence continues in the southeastern region along Zagros belt, in particular around the Lat=32.78^{o} N, Lon=50.10^{o} E and extends in a region between the two quiescences along the Zagros Mountains.

5. Conclusions

In this paper, the spatio-temporal evolution of seismicity in Northwestern Iran (Lat=30-38°N, Lon=43-53°E) has been analyzed by using the RTL algorithm. In particular, the presence of a possible seismic quiescences preceding the Mw=7.3 Sarpol Zahab earthquake in November 2017, a well-known precursor of strong earthquakes, has been investigated by retrospective analysis. RTL detects quiescences not only based on the number of the earthquakes, but also accounting for their energy and their spatial distribution. Since RTL algorithm analyzes the changes in background seismicity (i.e. with aftershocks removed), the declustering of the input catalog represents an essential step of the analysis. For this purpose, we used a quite novel approach, based on the nearest-neigbour distances between events in the space-time-energy domain (Zaliapin and Ben-Zion, 2013). Differently from classical window methods, this robust data-driven technique, while removing the clustered component, does not alter the features of inhomogeneous and possibly non-stationary background seismicity (Peresan and Gentili, 2019). Moreover, the method is characterized by a low number of parameters and it is not overly sensitive to the completeness of the earthquake catalog (Peresan and Gentili, 2018), all features that are relevant to allow for a possible prospective analysis of RTL seismicity patterns.

The application of RTL algorithm within an area centered at the mainshock epicenter evidences two significant quiescences: one deeper, with a duration 4-11 months, immediately preceding the Sarpol Zahab earthquake; the second one, lasting 9 months and preceding the other significant earthquake in the region, a Mw 5.7 earthquake occurred on November 2013 about 65 km away

from Sarpol Zahab earthquake. In order to understand if the evidenced quiescences can be related with these two strong and moderate earthquakes, we compared the obtained results with those reported in literature. Gentili (2010) investigated the seismicity by RTL on 12 earthquakes with ML>5 in Italy finding a quiescence in 92% of the cases, with a duration D varying from 0.6 to 3 years, and a lag s between the end of the quiescence and the earthquake occurrence in the range 0–2.9 years. These results were confirmed by the RTL analysis of seismicity before Central Italy earthquakes (Gentili et al., 2017), where a quiescence is detected with a duration D of one year and immediately preceding the earthquake (i.e. a lag s=0 years). Huang (2004), in a review on earthquakes with magnitude greater than 7 in Japan, Russia and Turkey, indicates a duration of 1–2.5 years and a beginning of the quiescence few years before the mainshock. The quiescence preceding the Mw 7.3 Sarpol Zahab 2017 earthquake, as well as the earlier Mw 5.7 2013 earthquake, have values of D and s comparable with the previous results.

In order to map RTL in space, an improved parameters-independent method for RTL evaluation has been proposed. The resulting map $\hat{Q}$ is a function of the geometric mean of maps obtained by RTL evaluation on the nodes of a grid, for different values of RTL parameters. This approach is more stable respect to the one used in literature, because it outlines only the parts of the map where a rather stable quiescence is detected, independently on parameters.

We computed the $\hat{Q}$ map from June 2017 to the midnight before the 7.3 Sarpol Zahab earthquake. The resulting map for Northwestern Iran (Lat=30-38°N, Lon=43-53°E), evidences a seismic quiescence anomaly extended throughout a broad NW-SE oriented region, corresponding to northern Zagros Mountains. In particular, a northern and a southern quiescence region have been detected. One, located to the north, evidences a significant seismic anomaly corresponding to the Sarpol Zahab earthquake; the second one is located in the southeastern part of the study region, in particular around the Lat=32.78^{o} N, Lon=50.10^{o} E. We also investigated how the RTL changes after the major earthquake, calculating the $\hat{Q}$ map from the day after the mainshock and up to the end of the available catalog (October 2018). We observed that the northern quiescence disappears immediately after the event, whereas the southeastern quiescence persists until the end of the data.

RTL has been already applied in many regions in the world (Russia, Greece, Japan, Turkey, Taiwan, China, Italy - e.g. Gentili, 2010 and references within). We believe that extending this analysis to Northwestern Iran, which is characterized by a peculiar tectonic and seismic regime, may help us to assess the generality of the related process of earthquake preparation. Moreover, the methodology applied in this study, aimed at quantitative identification of possible precursory quiescences, once systematically verified by retrospective analysis, may provide a relevant contribution towards a time-variable definition of the seismic hazard in Iran. Specifically, the focus can be placed on quiescent areas that are characterized by relatively high long-term probabilities and expected ground shaking (e.g. Talebi et al., 2017).

Acknowledgments

The data used in this study were extracted from the regional catalog of the Iranian Seismological Center (IGTU catalog), which is available at http://irsc.ut.ac.ir/bulletin.php; we are grateful to Saeed Soltani-Moghadam for assistance in data extraction. We thank Dr. Ilya Zaliapin for kindly supplying us the code of the nearest-neighbor method for clusters identification. This research is partly supported by the Civil Protection of the Friuli Venezia Giulia region (Italy).

References

Ambraseys, N., and C. Melville (1982). A History of Persian Earthquakes, Cambridge University Press. Cambridge, United Kingdom.

Bachmanov, D.M., Trifonov, V.G., Hessami, K.T., Kozhurin, A.I., Ivanova, T.P., Rogozhin, E.A., Hademi, M.C. and Jamali, F.H., 2004. Active faults in the Zagros and central Iran. Tectonophysics, 380(3-4), pp.221-241.

Baiesi, M., and M. Paczuski (2004), Scale-free networks of earthquakes and aftershocks. Phys. Rev. E, 69, 066106.

Chen C., and Y. Wu (2006), An improved region-time-length algorithm applied to the 1999 Chi-Chi, Taiwan earthquake, Geophys J Int, 166: 1 144-1 147.

Console, R., Montuori, C., Murru, M. (2000) Statistical assessment of seismicity patterns in Italy: Are they precursors of subsequent events? Journal of Seismology, 4, 435–449.

Davoudi N, Tavakoli H.R., Zare M., Jalilian A. (2018). Declustering of Iran earthquake catalog (1983–2017) using the epidemic-type aftershock sequence (ETAS) model. Acta Geophysica. https://doi.org/10.1007/s11600-018-0211-5.

De Santis, A.; Cianchini, G.; Qamili, E.; Frepoli, A. The 2009 L'Aquila (Central Italy) seismic sequence as a chaotic process. Tectonophysics 2010, 496, 44–52.

Di Giovambattista, R., and Y.S. Tyupkin (2000), Spatial and temporal distribution of the seismicity before the Umbria-Marche September 26, 1997 earthquakes, J. Seismol. 4, 589–598.

Di Giovambattista, R., and Y. S. Tyupkin (2004), Seismicity patterns before the M = 5.8 2002, Palermo (Italy) earthquake: seismic quiescence and accelerating seismicity, Tectonophysics 384, 243–255.

Gentili, S. (2010), Distribution of Seismicity Before the Larger Earthquakes in Italy in the Time Interval 1994–2004, Pure Appl. Geophys., 167, 933–958.

Gentili, S., and G. Bressan (2007), Seismicity patterns before MD C 4.1 earthquakes in the Friuli-Venezia Giulia (northeasternItaly) and western Slovenia areas, Bollettino di Geofisica Teorica ed Applicata, 48, 33–51.

Gentili, S., Di Giovambattista, R, Peresan, A., 2017. Seismic quiescence preceding the 2016 central Italy earthquakes. Physics of the Earth and Planetary Interiors 272, 27-33.

Grassberger P., and Procraccia I., 1983. Measuring the strangeness of strange attractors. Physica D 9: 189–208.

Gutenberg, B., and Richter, C. F., 1944. Frequency of earthquakes in California. Bulletin of the Seismological Society of America 142, 185–188.

Hessami, F., F. Jamali, and H. Tabassi (2003). Major Active Faults of Iran, International Institute of Earthquake Engineering and Seismology (IIEES), Tehran, Iran.
International Institute of Earthquake Engineering and Seismology (IIEES), 2017. Preliminary report of Azgale earthquake (in Persian).

Huang, Q. (2004), Seismicity pattern changes prior to large earthquakes-An approach of the RTL algorithm. Terres. Atmos. Oceanic Sci. 15, 469–491.

Huang, Q. (2006), Search for reliable precursors: A case study of the seismic quiescence of the 2000 western Tottori prefecture earthquake, J. Geophys. Res. 111, B04301, doi:10.1029/2005JB003982.

Huang, Q. (2008), Seismicity changes prior to the Ms8.0 Wenchuan earthquake in Sichuan, China, Geophys. Res. Lett. 35, L23308, doi:10.1029/2008GL036270.

Huang Q. H., and X. Ding (2012), Spatiotemporal variations of seismic quiescence prior to the 2011 M 9.0 Tohoku earthquake revealed by an improved Region-Time-Length algorithm, Bull. Seismol. Soc. Am. 102(4):1878–1883.

Huang, Q., Öncel, A. O., Sobolev, G. A. (2002), Precursory seismicity changes associated with the Mw= 7.4 1999 August 17 Izmit (Turkey) earthquake, Geophys. J. Int. 151, 235– 242.

Huang, Q., Sobolev, G. A., Nagao, T. (2001), Characteristics of the seismic quiescence and activation patterns before the M = 7.2 Kobe earthquake, January 17, 1995, Tectonophysics, 337, 99–116.

IRSC: The Iranian Seismological Center (http://irsc.ut.ac.ir/bulletin.php, last accessed October 2018).

Mirzaei, N., Gao, M. and Chen, Y.T., 1999. Delineation of potential seismic sources for seismic zoning of Iran, J. Seismol., 3, 17-30.

Main, I. G., and Meredith, P. G. (1989), Classification of earthquake precursors from a fracture mechanics model. Tectonophysics, 167, 273-283.

Mignan, A. (2008), The Non-Critical Precursory Accelerating Seismicity Theory (NC PAST) and limits of the power-law fit methodology, Tectonophysics, 452, 42–50.

Mignan, A., and R. Di Giovambattista (2008), Relationship between accelerating seismicity and quiescence, two precursors to large earthquakes, Geophys. Res. Lett., 35, L15306, doi:10.1029/2008GL035024.

Nagao, T., A. Takeuchi, and K. Nakamura (2011), A new algorithm for the detection of seismic quiescence: introduction of the RTM algorithm, a modified RTL algorithm, Earth Planets Space, 63, 315–324, 2011. 10.5047/eps.2010.12.007.

Nissen, E., Tatar, M., Jackson, J.A. & Allen, M.B., 2011. New views on earthquake faulting in the Zagros fold-and-thrust belt of Iran, Geophys.J. Int., 186(3), 928–944.

Palano, M., Imprescia, P., Agnon, A. and Gresta, S., 2018. An improved evaluation of the seismic/geodetic deformation-rate ratio for the Zagros Fold-and-Thrust collisional belt. Geophysical Journal International.

Peresan, A., Gentili, S., 2018. Seismic clusters analysis in Northeastern Italy by the nearest-neighbor approach Physics of the Earth and Planetary Interiors, 274, 87-104.

Peresan, A., Gentili, S., 2019. Identification and characterization of earthquake clusters: a comparative analysis for selected sequences in Italy and adjacent regions, Bollettino di Geofisica Teorica ed Applicata, in press.

Pu, H. (2018) Spatial and Temporal Characteristics of the Microseismicity Preceding the 2016 M_L 6.6 Meinong earthquake in southern Taiwan, Pure Appl. Geophys., 175, 2077-2091.

Scholz, C. H., (1988) Mechanisms of Seismic Quiescences PAGEOPH, 126, 701-718.

Shahvar,M. P.,M. Zare, and S. Castellaro (2013).A unified seismic catalog for the Iranian Plateau (1900–2011), Seismol. Res. Lett. 84, no. 2, 233–249.

Sobolev, G. A. (1995) Fundamental of Earthquake Prediction. Moscow: Electromagnetic Research Centre, 162 p.

Sobolev G.A., Q.Huang, T.Nagao. (2002) Phases of earthquake's preparation and by chance test of seismic quiescence anomaly, Journal of Geodynamics, 33, 413-424.

Sobolev, G. A., and Y. S Tyupkin (1996), New method of intermediate term earthquake prediction. In European Seismological Commission XXV General Assembly Seismology in Europe, Reykjavik, Iceland, 9–13 September 1996, pp. 229–234.

Sobolev, G. A., Tyupkin Y. S. (1997), Low seismicity precursors of large earthquakes in Kamchatka,. Volc. Seis. 18, 433-446.

Sobolev, G.A., Tyupkin, Yu.S., 2000. An analysis of the seismic energy emission process during formation of the main rupture in laboratory experiments on destruction of rocks and before large earthquakes. Fiz. Zemli N2, 44–55 (in Russian).

Talebi, M., Zare, M., Madahi-Zadeh, R., & Bali-Lashak, A. (2015). Spatial-temporal analysis of seismicity before the 2012 Varzeghan, Iran, Mw 6.5 earthquake. Turkish Journal of Earth Sciences, 24(3), 289–301.

Talebi M., Zare M., Peresan A., Ansari A. (2017). Long-Term Probabilistic Forecast for M≥ 5.0 Earthquakes in Iran. Pure and Applied Geophysics 4 (174), 1561-1580. DOI: 10.1007/s00024-017-1516-z.

Tchalenko, J.S., Braud, J., 1974. Seismicity and structure of the Zagros (Iran): the Main Recent Fault between 33j and 35jN. Philos. Trans. R. Soc. Lond. 277, 1– 25.

Tzanis, A.; Vallianatos, F. Distributed power-law seismicity changes and crustal deformation in the SW Hellenic Arc. Nat. Hazards Earth Syst. Sci. 2003, 3, 179–195.

Varini E., Peresan A., Rotondi R., Gentili S. (2018). Space-time earthquake clustering: nearest-neighbor and stochastic declustering methods in comparison. Proceedings of the "SIS2018: 49th Scientific Meeting of the Italian Statistical Society", 20-22 June Palermo (Italy). http://meetings3.sis-statistica.org/index.php/sis2018/49th/paper/viewFile/1543/144

Walpersdorf, A., et al., 2006. Difference in the GPS deformation pattern of North and Central Zagros (Iran), Geophys. J. Int., 167(3), 1077–1088.

Wen, Y., C. Chen, Y. Wu, C. Chan, Y.Wang, and Y. Yeh (2016), Spatiotemporal investigation of seismicity and Coulomb stress variations prior to the 2010 ML 6.4 Jiashian, Taiwan earthquake, Geophys. Res. Lett., 43, 8451–8457.

Wiemer, S., 2001. A software package to analyze seismicity: ZMAP. Seismol Res Lett 72: 373–382.

Wiemer, S., Wyss, M. (1994), Seismic quiescence before the Landers (M=7.5) and Big Bear (M=6.5) 1992 earthquakes, Bull. Seism. Soc. Am. 84, 900-916.

Wyss, M., Console, R., and Murru M. (1997), Seismicity Rate Change Before the Irpinia (M = 6.9) 1980 Earthquake. Bull. Seismol. Soc. Am. ,87, 318-326.

Wyss, M., Habermann, R. E. (1988), Precursory seismic quiescence. Pure and Applied Geophysics 126, 701-718.

Yang, Y. H., Hu, J. C., Yassaghi, A., Tsai, M. C., Zare, M., Chen, Q., & Kamranzad, F. (2018). Midcrustal Thrusting and Vertical Deformation Partitioning Constraint by 2017 M w 7.3 Sarpol Zahab Earthquake in Zagros Mountain Belt, Iran. Seismological Research Letters.

Zaliapin, I., A. Gabrielov, H. Wong, and V. Keilis-Borok (2008), Clustering analysis of seismicity and aftershock identification, Phys. Rev. Lett., 101.

Zaliapin, I. and Y. Ben-Zion (2013), Earthquake clusters in southern California I: Identification and stability, J. Geophys. Res., 118(6), 2847-2864, doi:10.1002/jgrb.50179.

Zare, M., H. Amini, P. Yazdi, K. Sesetyan, M.B. Demircioglu, D. Kalafat, M. Erdik, D. Giardini, M. Asif Khan and N. Tsereteli (2014). Recent developments of the Middle East catalog, J. Seismol., 18 (3); doi:10.1007/s10950-014-9444-1.

SUPPLEMENTARY FIGURE

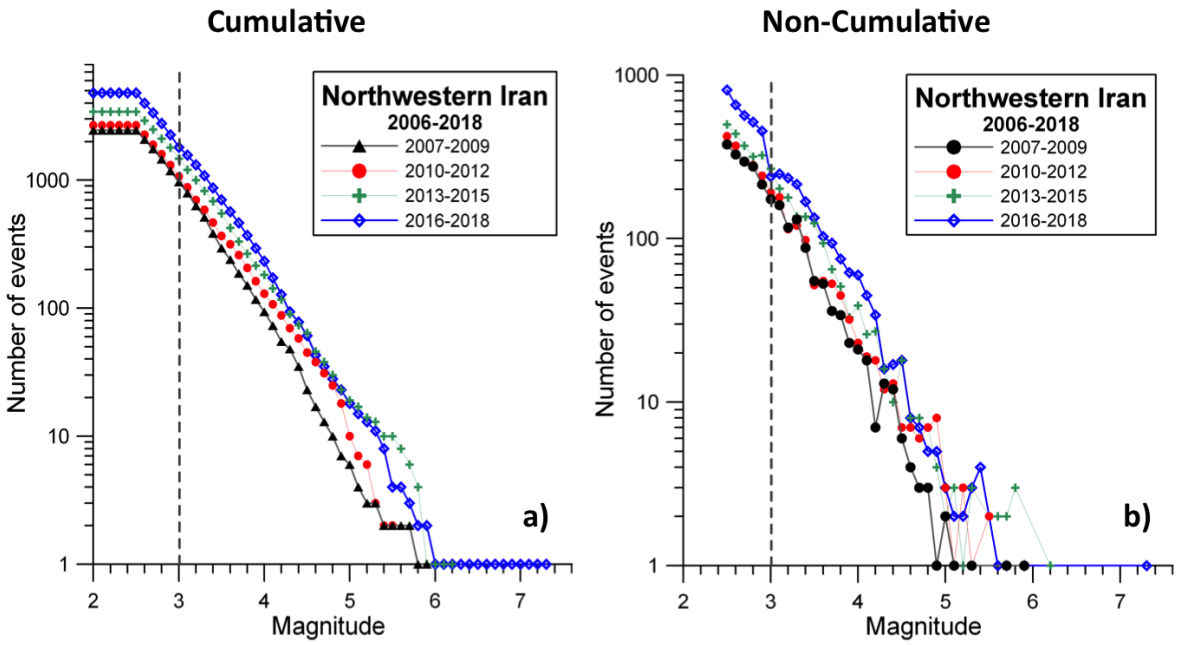

Figure S1 - Temporal analysis of completeness for IGTU earthquake data in Northwestern Iran: a) cumulative and b) non-cumulative distributions of the number of events vs magnitude, obtained considering four consecutive time-windows.